Electronic Supplementary Material (ESI) for Materials Horizons.

Supplementary Information

3D-Printing Method of Fabrication for Metals, Ceramics, and Multi-Materials through Universal Self-Curable Technique for Robocasting

Danwei Zhang[a‡], Win Jonhson[a‡], Tun Seng Herng[a], Yong Quan Ang[a], Lin Yang[a], Swee Ching Tan[a], Erwin Peng[a]*, Hui He[b]*, Jun Ding[a]*

Ms. Zhang Danwei, Mr Win Jonhson, Dr. Herng Tun Seng, Mr Ang Yong Quan, Dr. Yang Lin, Prof. Tan Swee Ching, Dr. Erwin Peng, Prof. Ding Jun

[a]. *Department of Materials Science and Engineering, Faculty of Engineering, National University of Singapore, Singapore, Singapore*

Dr. He Hui

[b].*Key Laboratory of Low-grade Energy Utilization Technologies and System (Chongqing University), Ministry of Education, Chongqing 400044, China*

‡ These authors contribute equally to this work.

** Corresponding authors.*

Section 1. Experimental Section.

Materials:

Ethylene glycol (EG), diethylene glycol (DEG), poly(ethylene glycol) diglycidyl ether (PEGDE Mn 500), strontium carbonate ($SrCO_3$), nickel oxide (NiO), zinc oxide (ZnO), iron oxide (Fe_2O_3), yttria (Y_2O_3), copper oxide (CuO), niobium oxide (Nb_2O_5), titanium dioxide (TiO_2) and silicon nitride (Si_3N_4) were obtained from Sigma Aldrich, Singapore. Silicon carbide (SiC) was obtained from Goodfellow. EpoThin 2 Resin (ETR) and EpoThin 2 Hardener (ETH) were obtained from AccuMet Instruments Pte. Ltd, Singapore. Al-doped ZnO (AZO) nanopowders and copper nanopowders were purchased from Skyspring Nanomaterials, US. White-colored and blue-colored yttria-stabilized zirconia powders (denoted as CY3Z-RA and blue-YZe respectively) and alumina powder (E440 grade) were kindly provided by Saint Gobain Research Shanghai, China.

Ferrite Powders Preparation:

To obtain strontium ferrite powders, 1 mol of $SrCO_3$ to 6 mol of Fe_2O_3 were homogenized using Fritsch P6 premium line planetary ball mill with stainless steel milling jars and grinding balls at high speed. To obtain nickel-zinc ferrite powders, 0.5 mol of NiO to 0.5 mol of ZnO to 1 mol of Fe_2O_3 were homogenized using Fritsch P6 premium line planetary ball mill with stainless steel milling jars and grinding balls at high speed.

Self-Curable Ceramic/Metal Paste Preparation:

Ceramic/metal powders were homogenized with plasticizers (e.g., EG, DEG) and PEGDE in a mortar and pestle for at least 10 minutes. Once homogenized, ETH was added into the slurry to obtain a shear-thinning paste for the robocasting process.

Robocasting of Self-Curable Ceramic/Metal Paste:

The self-curable epoxide-amine curing pastes were extruded using Regenhu 3DDiscovery (Fribourg, Switzerland) via compressed air. Tapered stainless steel nozzles (purchased from Able Industrial Engineering Pte. Ltd., Singapore) of inner diameter ranging from 270 μm to 410 μm were used in the printing process.

Post-Printing Heat Treatment:

The post-printing curing process can be done by allowing it to cure at room temperature for several hours. To accelerate the curing process, heating of temperatures between 50°C-100°C can be harnessed through substrate heating, chamber/printer heating environment, using an external source

(infrared, heat, air), etc. To allow for complete plasticizer evaporation, the structures are subjected to thermal heating of temperatures between 100^{o}C to 250^{o}C for a few hours in a Carbolite Ashing Furnace AAF1100 (UK). Debinding (temperatures between 300^{o}C -600^{o}C) and sintering (1200^{o}C -1450 ^{o}C) of ceramic structures took place in a Carbolite High-Temperature Box Furnace HTF18/4 (UK). Ramping rate of 1^{o}C/min was used.

Section 2. Refractive Index and Absorption Coefficients of Ceramics and Metals.

Material	Refractive Index (*n*)	Absorption Coefficient (α, cm^{-1})
Aluminum Oxide, (α-alumina)	1.761	-
Tin oxide, (cassiterite)	2.006	-
Barium Titanate, (tetragonal)	2.40	-
Iron (II, III) Oxide, (magnetite)	2.42	-
Silicon Carbide, (wurtzite)	2.654	-
Iron (III) Oxide, (hematite)	2.91	-
Copper	0.6366	5.9526×10^5
Iron	2.9304	$6.4149e \times 10^5$
Nickel	1.9648	8.2019×10^5

Fig. S1. List of a few common ceramics and metals' refractive index and absorption coefficient. [1-3]

High refractive index and absorption coefficients of materials, both ceramics and metals, impede the curing depth of these materials' feedstock. Aluminum oxide is a chosen ceramic material to be used in photocurable-based formulations[4, 5] compared to ceramics like silicon carbide and iron oxide (see **Fig. S1**). Metals, on the other hand, have high absorption coefficients. As a result, the curing depth of the photocurable matrix will be severely opposed. The proposed technique of using a self-curable polymer matrix would be able to mitigate this issue. Ceramic and metal structures can be cured using the proposed technique without any hindrance on their refractive index and absorption coefficients as the structures are cured due to the chemical reaction between PEGDE and ETH.

Section 3. Robocasting Set-up.

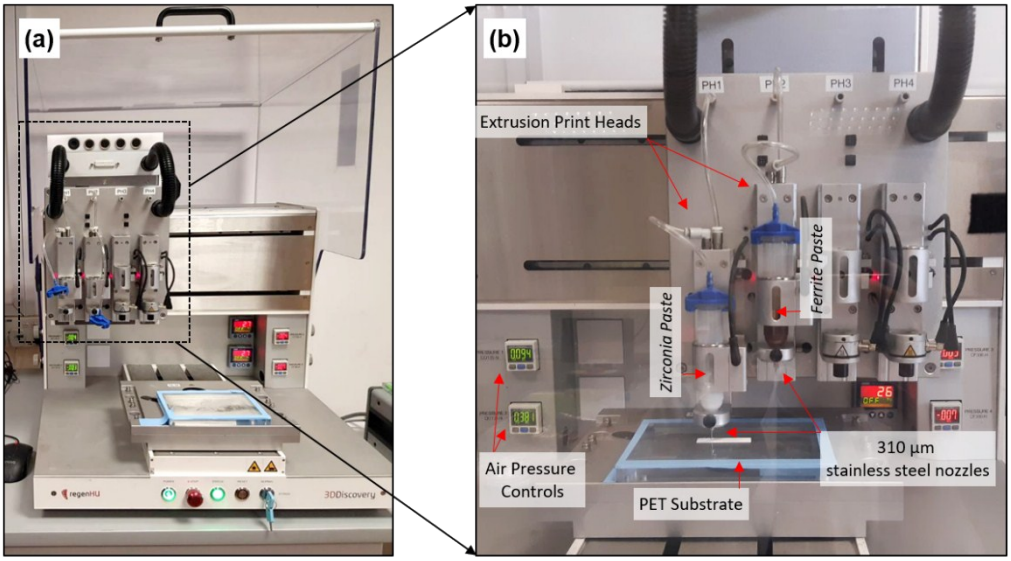

Fig. S2. Robocasting Set-up using Regenhu 3DDiscovery Bioprinter. (a) Regenhu 3DDiscovery Bioprinter. (b) Robocasting Set-up details.

A Regenhu 3DDiscovery Bioprinter is shown in Fig. S2a. The ceramic and metal pastes were extruded using Regenhu 3DDiscovery (Fribourg, Switzerland) via compressed air. Dual print heads can be utilized for multi-material printing. Stainless steels nozzles of inner diameter 310 µm were used as shown in **Fig. S2b**. A polyethylene terephthalate (PET) film is used as the substrate surface. According to the viscosity of the paste, printing speed and air pressure can be tailored through BioCAD™ software and pressure knobs respectively.

Section 4. Effects on Resultant Sintered Structures Due to Absence of Plasticizers.

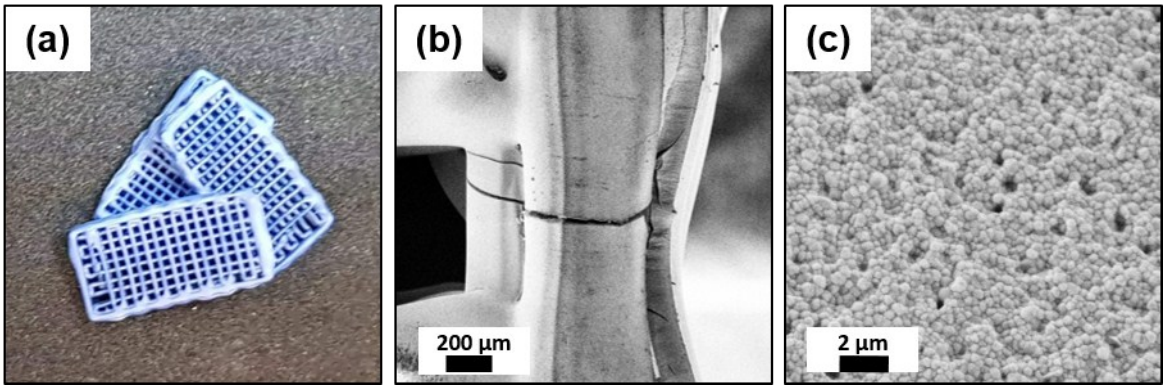

Fig. S3. Sintered blue-colored zirconia at 1400°C for 5 hours using a commercial Epoxide-amine pack. (a) Digital image sintered blue-colored zirconia structure, (b) and (c) SEM images showing cracks and pores in sintered structure.

Dispersion is a challenging field in the ceramics research area[6-8]. The proposed low molecular weight plasticizers also act as diluents, allowing for a stable and well-dispersed media suitable for extrusion printing[5]. The zirconia paste used to print zirconia structures (without the use of low molecular weight plastivizers) as shown in Fig. S3a has a solid loading of 20 vol %. This is relatively low if dense and crack-free structures were to be obtained. In comparison, if ethylene glycol (EG) would be added into the slurry, a zirconia printing paste of 40 vol % solid loading would be attainable.

Besides acting as a dispersing agent, EG also allows for low-temperature plasticizer evaporation. This minimizes the overall high volume of organic burn-off of the Green-Body. As a result of the three-step heat treatment process, resultant crack-free and dense sintered structures can be realized as shown in Fig. 2f. In Fig. S3b-c, no plasticizers were added. Commercial ETR and ETH resins were solely used. The sintered structures as shown in Fig. S3b-c show cracks and pores after using the same heat treatment process for obtaining sintered structures in this paper. To achieve crack-free and dense sintered structures, without the use of plasticizers, a slower ramping rate and longer dwelling duration at high temperatures are required. This would result in a poor and inefficient process and production.

Section 5. Self-Curing Approaches and Secondary Shaping Approaches

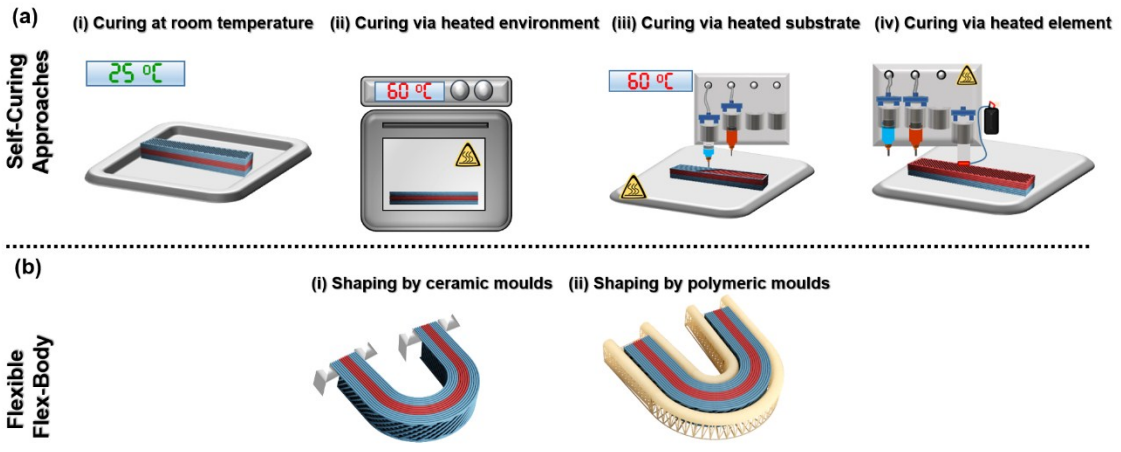

Fig. S4. Approaches to form flexible metal/ceramic 3D printed structure. (a) Self-curing approaches. (i) Curing at room temperature, (ii) curing in oven at elevated temperatures after printing, (iii) accelerated curing through heated substrate bed and (iv) accelerated curing through heating filament. (b) Secondary shaping by utilizing (i) porous polymeric mold and (ii) ceramic molds.

Self-curing of the as-printed structures can happen without an external source such as UV or heat. Given sufficient time, the structure can be cured at room temperature (see **Fig. S4a(i)**). To accelerate the curing, the structure can be heated to a mild temperature (about 60^{o}C-80^{o}C) (see **Fig. S4a(ii)**). The substrate bed can also be heated or a heating filament can be employed (see **Fig. S4a(iii-iv)**).

To achieve secondary shaping, two methods are employed[5]. Both ceramic and polymeric molds can be used (see **Fig. S4b**). These molds are used to obtain a rigid Green-Body after plasticizer evaporation at lower temperatures (<250^{o}C).

Section 6. Formulation of Nickel-Zinc Ferrite Paste for Robocasting.

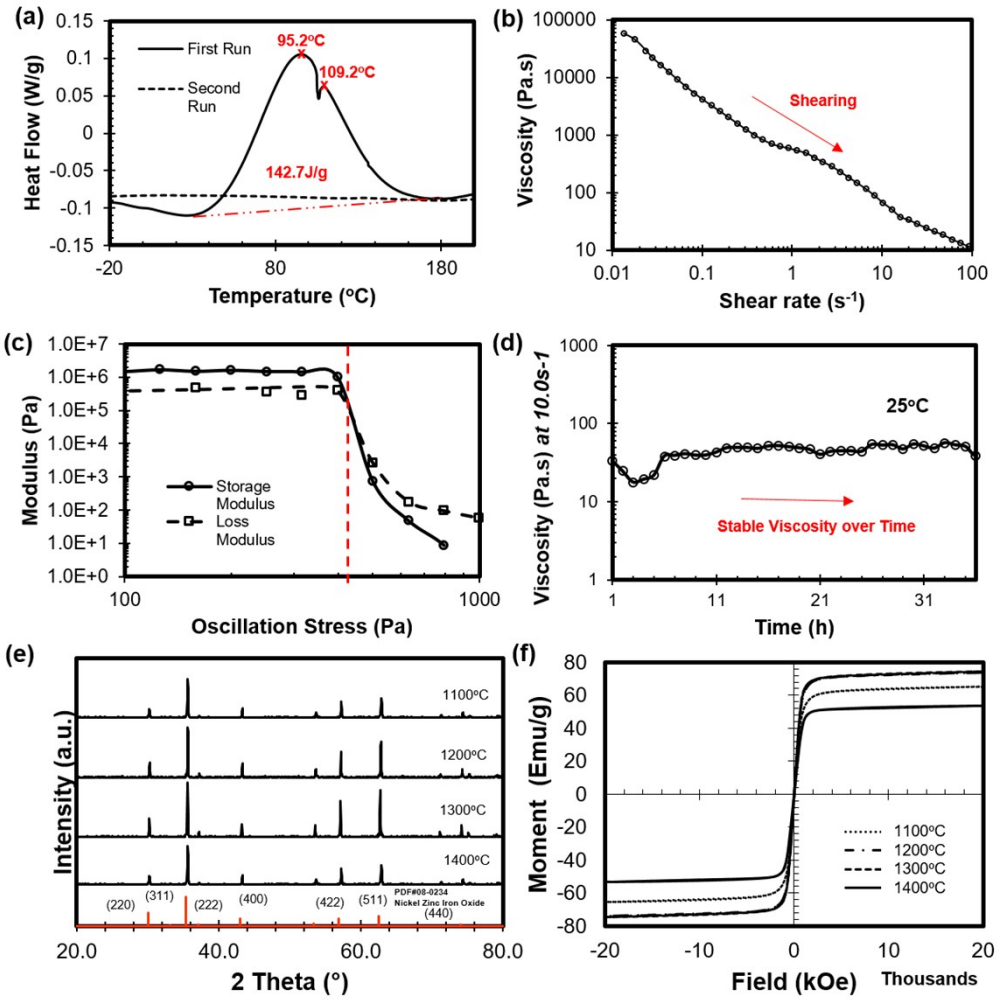

Fig. S5. Characterization of nickel-zinc ferrite paste. (a) DSC measurement of epoxide-amine reagents used for nickel-zinc ferrite paste. The normalized heat flow was plotted against temperature. (b) Rheological measurement of nickel-zinc ferrite paste's apparent viscosity as a function of shear rate. (c) Nickel-zinc ferrite paste's shear storage modulus and loss modulus as a function of oscillation stress. (d) Stability of Pack A over time. (e) XRD of sintered nickel-zinc ferrite structure over different sintering temperatures at a constant duration of 5 hours. (f) Magnetic moment of sintered nickel-zinc ferrite as a function of temperature.

PEGDE and ETH were mixed and left to stand at ambient conditions for 15 minutes before DSC experiment started. The heating rate was 5^{o}C/min and measurements were conducted in a nitrogen atmosphere from -30^{o}C to 200^{o}C. The absence of the exothermic curves from the second DSC run, as shown in **Fig. S5a**, confirms the polymerization reaction between 0.20:1 volume ratio of ETH and PEGDE used in formulating nickel-zinc ferrite pastes for robocasting. The heat of cure, given under the area of the exothermic peaks, is 142.7 J/g. From the absence of exothermic curves in the second run measurement, it was deduced that the epoxide-amine curing system was completely polymerized after the first run. From **Fig. S5b**, the optimized nickel-zinc ferrite paste has a shear thinning behavior which is suitable for robocasting purposes. The shear yield stress, given by the intersection between the storage and loss moduli curves, is ~400Pa as shown in **Fig. S5c**. The printing paste can be stored in a two-pack system to increase its shelf life. Pack A consists of nickel-zinc ferrite powders homogenized with DEG and PEGDE while Pack B consists of ETH. The stability of Pack A in atmospheric conditions (25^{o}C) as a function of time can be seen in **Fig. S5d**. Nickel-zinc ferrite samples are subjected to various sintering temperatures from 1100˚C to 1400˚C for 5 hours and characterized with a Vibrating-Sample Magnetometer (VSM) and X-ray diffractometer (XRD) to investigate the magnetic properties and phase transformation respectively. The presence of $Ni_{0.5}Zn_{0.5}Fe_2O_4$ phase (JCPDS #08-0234) is detected in sintering temperatures of 1100^{o}C to 1400^{o}C is shown in **Fig. S5e**. As presented in **Fig. S5f**, the highest magnetic saturation (Ms) = 74.4 emu/g is obtained at a sintering temperature of 1300˚C for 5 hours.

Section 7. Fabrication of Ceramic and Metal Structures through Robocasting Using Self-Curable Technique.

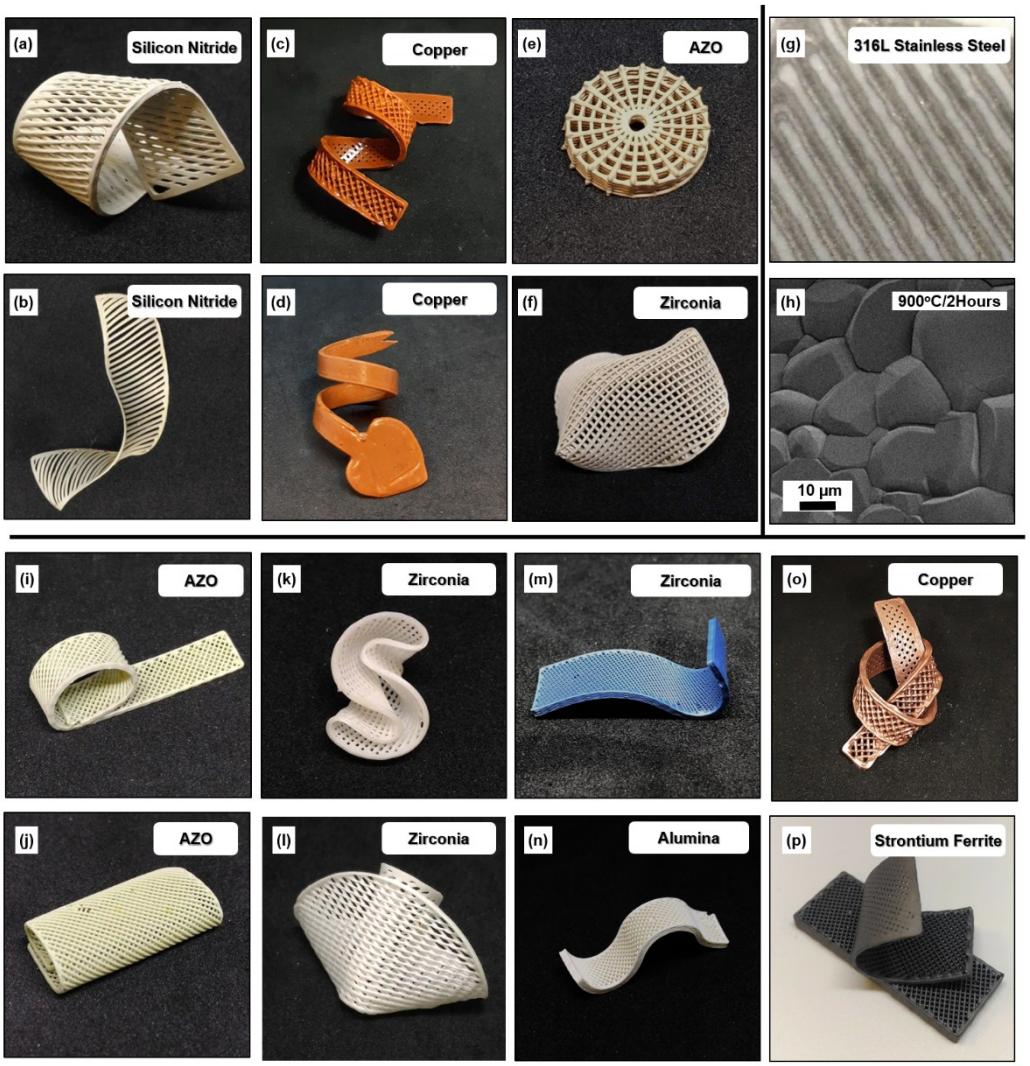

Fig. S6. Digital images of sintered structures fabricated using self-curing technique for robocasting. (a-f) Digital images of several Green-Bodies which has undergone secondary shaping, (g-h) 316L stainless steel sintered under nitrogen conditions at 900°C for 2 hours, (i-p) Digital images of Sintered-Bodies which have retained the shape after sintering and achieving densification.

Colored ceramic materials usually have a high refractive index[8-10]. These materials include AZO, ferrites and colored ceramics (such as blue-colored zirconia). With the proposed technique, a wide array of ceramic and metal materials can be cured and shaped after printing (see **Fig. S6**). This secondary shaping complements the current 3D printing technologies and adds an additional

dimension to the complexity of the structure easily (see **Fig. 3**). Metals can also be cured and shaped using the self-curable technique. As an example in **Fig. S6g-h**, 316L stainless steel can be cured and sintered to be dense in 900^{o}C for 2 hours under nitrogen atmosphere. The limitless possibilities of printing ceramics and metals open up multi-materials printing opportunities that can realize integrated and functional structures in the near future.

Section 8. Liquid Phase Sintering of (β-phase) Silicon Carbide Structures.

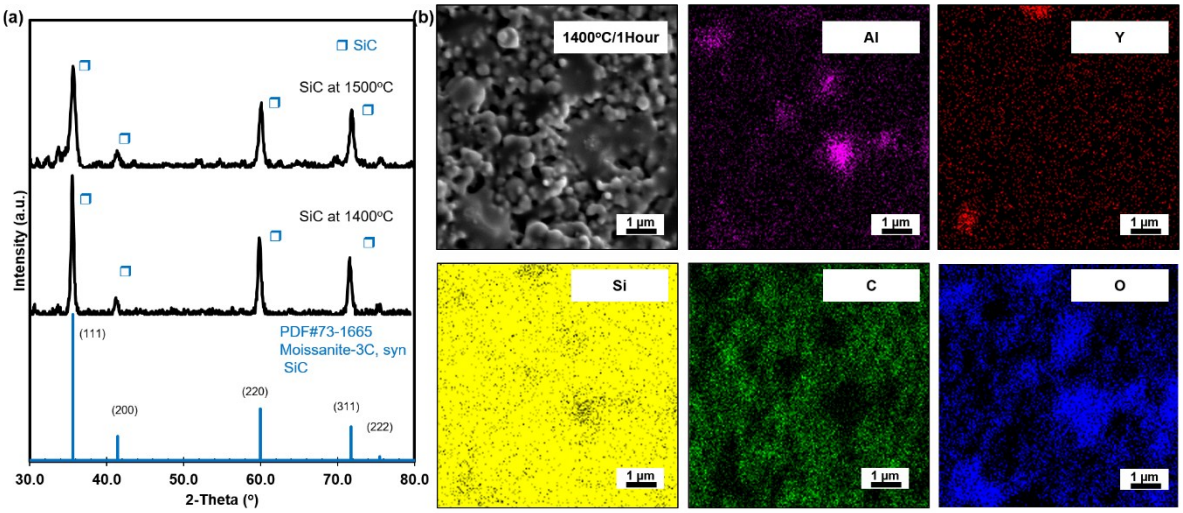

Fig. S7. Sintering of (β-phase) silicon carbide. (a) XRD patterns of Silicon Carbide (SiC) Sintered-Body at 1400°C for 5 hours and 1500°C for 5 hours under a nitrogen atmosphere. (b) EDX mapping showing the liquid melt sintering process occurring at 1400°C at 1 hour with sintering additives of alumina (Al_2O_3) and yttria (Y_2O_3).

In order to obtain dense (β-phase) silicon carbide (SiC) structures, alumina (2.0 wt %) and yttria 8.0 wt %) were utilized as sintering aids to assist in microstructural formation[11-13]. At high temperatures, these additives form a liquid phase between SiC particles, forming a high diffusivity path for densification to occur[14]. **Fig. S7a** shows the XRD patterns of SiC sintered at 1400°C and 1500°C for 5 hours correspond to that in JCPDS #73-1665. **Fig. S7b** shows the liquid phase sintering process at 1400°C for 1 hour where alumina and yttria formed melt pools for densification of SiC particles.

Section 9. Microstructural Analysis of Alumina-Doped Zinc Oxide with Sintering Temperature.

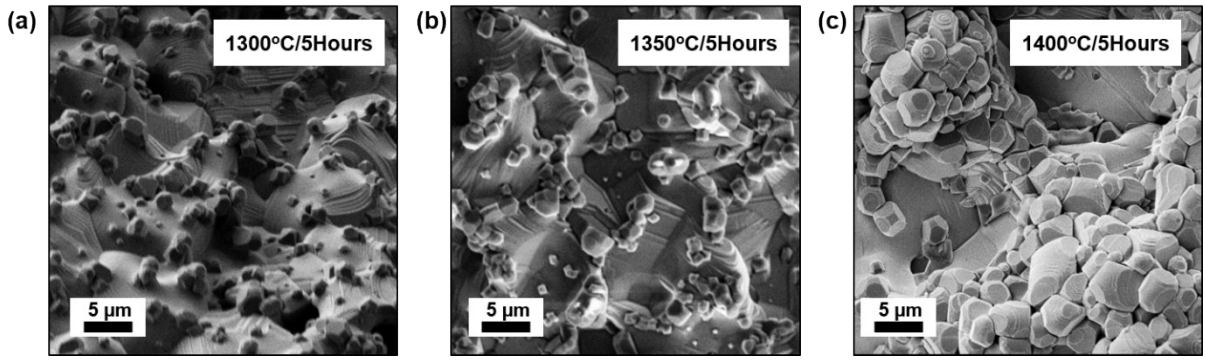

Fig. S8. Sintering of dense alumina-doped zinc oxide (AZO). SEM images showing (a) AZO sintered at 1300°C for 5 hours, (b) AZO sintered at 1350°C for 5 hours, (c) AZO sintered at 1400°C for 5 hours.

Alumina-doped zinc oxide (AZO) is a ceramic material that is able to conduct electricity when sintered at high temperatures[15]. Applications for the usage of AZO include solar cell applications[16-18] and optoelectronic devices[19]. The microstructures of AZO was investigated as a function of sintering temperature. From 1300°C to 1400°C (keeping sintering duration constant at 5 hours), sintered AZO structures were able to achieve full densification as shown in **Fig. S8a-c**. However, at 1400°C (with sintering duration of 5 hours), there are great variations in grain sizes. Therefore, sintering temperatures of 1300°C to 1350°C were preferred.

Section 10. Microstructural Analysis of Doped-Alumina with Sintering Temperature.

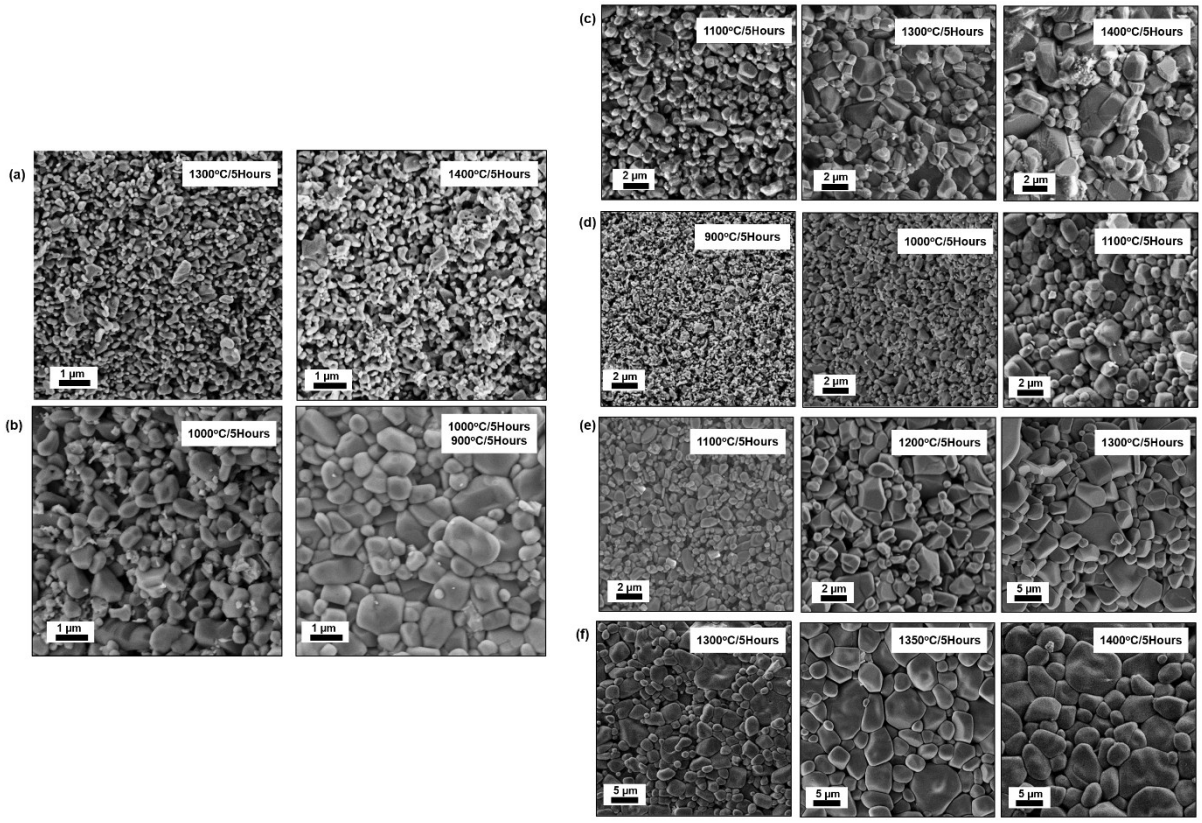

Fig. S9. Sintering of Alumina with the addition of dopants to lower sintering temperature. (a) (From left to right) Pure alumina (E440 grade) sintered at 1300°C for 5 hours showing porosity, pure alumina (E440 grade) sintered at 1400°C for 5 hours showing porosity, (b) Effects of annealing shown to contribute to dense microstructure. Sintering additives of copper oxide, titanium dioxide, and niobium oxide were employed. (c) Effects of grain size and density of microstructure with increasing temperature when copper oxide and titanium dioxide are added as sintering additives. (From left to right) Sintering temperature of 1100°C, 1300°C and 1400°C for 5 hours was employed. d) Effects of grain size and density of microstructure with increasing temperature when copper oxide, titanium dioxide, and niobium oxide are added as sintering additives. (From left to right) Sintering temperature of 900°C, 1000°C and 1100°C for 5 hours was employed. (e) Effects of grain size and density of microstructure with increasing temperature when manganese oxide is added as sintering additive. (From left to right) Sintering temperature of 1100°C, 1200°C and 1300°C for 5 hours was employed. (f)

Effects of grain size and density of microstructure with increasing temperature when titanium dioxide and niobium oxide are added as sintering additives. (From left to right) Sintering temperature of 1300^{o}C, 1350^{o}C and 1400^{o}C for 5 hours was employed.

To investigate the possibility of multi-materials printing, a structural ceramic (alumina) and a functional ceramic (AZO) are explored. From **Fig. S8**, the optimal sintering temperature of AZO is between 1300^{o}C and 1350^{o}C. It is therefore important to match the sintering temperature of alumina to that of AZO. From **Fig. S9a**, sintering alumina at 1300^{o}C to 1400^{o}C will result in a porous structure. Therefore, some methods can be employed to lower the sintering temperature of alumina. One way is through the usage of multi-stage sintering[20]. In **Fig. S9b**, alumina (doped with copper oxide, titanium dioxide, and niobium oxide) was investigated for the effects of multi-stage sintering. At 1000^{o}C, the structure's SEM image shows pores within its microstructural matrix. Cooling down the sample to room temperature and heating it to 900^{o}C resulted in a denser microstructure. However, this heat treatment method is time-consuming. When integrated with other materials, AZO faces the issue of abnormally large grains when multi-stage sintering is used (see **Fig. S9b**). The other method to lower the sintering temperature of alumina for densification is through the use of sintering additives[21]. Sintering additives such as copper oxide (CuO), titanium dioxide (TiO_2) and niobium oxide (Nb_2O_5) can be used as effective dopants to lower the sintering temperature of alumina[22]. From **Fig. S9c-S9e**, a combination of sintering additives is used across various sintering temperatures. However, they show (i) large variations in grain sizes and (ii) porosity at the targeted sintering temperature of between 1300^{o}C-1350^{o}C. Furthermore, utilizing CuO as a sintering additive would render the structure to have a black color finishing. As a result, TiO_2 and Nb_2O_5 were chosen as sintering additives for alumina. **Fig. S9f** shows the capability of doped alumina with TiO_2 (2.0 wt %) and Nb_2O_5 (4.0 wt %) to be dense at sintering temperatures of between 1300^{o}C-1350^{o}C.

Supporting Information References

1. C. B. Carter and M. G. Norton, *Ceramic materials: science and engineering*, Springer, New York, NY, 2nd edn., 2013.
2. P. B. Johnson and R. W. Christy, *Physical Review B*, 1972, **6**, 4370-4379.
3. P. B. Johnson and R. W. Christy, *Physical Review B*, 1974, **9**, 5056-5070.
4. Y. de Hazan, M. Thänert, M. Trunec and J. Misak, *Journal of the European Ceramic Society*, 2012, **32**, 1187-1198.
5. D. Zhang, E. Peng, R. Borayek and J. Ding, 2019, **29**, 1807082.
6. J. Texter, *Nanoparticle dispersion: Challenges and solutions*, 2004.
7. X. Li, H. Zhong, J. Zhang, Y. Duan, H. Bai, J. Li and D. Jiang, *International Journal of Applied Ceramic Technology*, 2019, **0**.
8. B. Johnson and A. K. Walton, *British Journal of Applied Physics*, 1965, **16**, 475-477.
9. P. Dararutana, J. Dutchaneephet, P. Chetanachan, P. Wathanakul and N. Sirikulrat, *Advanced Materials Research*, 2008, **55-57**, 601-604.
10. R. E. Treharne, A. Seymour-Pierce, K. Durose, K. Hutchings, S. Roncallo and D. Lane, *Journal of Physics: Conference Series*, 2011, **286**, 012038.
11. K. Cai, B. Román-Manso, J. E. Smay, J. Zhou, M. I. Osendi, M. Belmonte and P. Miranzo, *Journal of the American Ceramic Society*, 2012, **95**, 2660-2666.
12. J. Marchi, J. Bressiani and A. Bressiani, *Sintering of Silicon Carbide Ceramics with Additives Based on the (Y2O3-Al2O3-SiO2) System*, 2006.
13. J. Zhang, D. Jiang, Q. Lin, Z. Chen and Z. Huang, *Journal of the European Ceramic Society*, 2013, **33**, 1695-1699.
14. Y. Yang, F. Han, W. Xu, Y. Wang, Z. Zhong and W. Xing, *Ceramics International*, 2017, **43**, 3377-3383.
15. K. H. Kim, K. C. Park and D. Y. Ma, *Journal of Applied Physics*, 1997, **81**, 7764-7772.
16. W. J. Jeong, S. K. Kim and G. C. Park, *Thin Solid Films*, 2006, **506-507**, 180-183.
17. N. Sun, G. Fang, P. Qin, Q. Zheng, M. Wang, X. Fan, F. Cheng, J. Wan and X. Zhao, *Solar Energy Materials and Solar Cells*, 2010, **94**, 2328-2331.
18. S. Sutthana, N. Hongsith and S. Choopun, *Current Applied Physics*, 2010, **10**, 813-816.
19. W. Li, Y. Qiu, L. Zhang, L. Jiang, Z. Zhou, H. Chen and J. Zhou, *Biosens Bioelectron*, 2016, **79**, 500-507.
20. C.-T. Hu and W.-C. Chiou, *Metallurgical and Materials Transactions B*, 1998, **29**, 1069-1076.
21. L. A. Xue and I. W. Chen, *Journal of the American Ceramic Society*, 1991, **74**, 2011-2013.
22. K. Shigeno, H. Katsumura, H. Kagata, H. Asano and O. Inoue, *Key Engineering Materials - KEY ENG MAT*, 2006, **320**, 181-184.